The interaction of Indian monsoon depressions with northwesterly mid-level dry intrusions

Article

Accepted Version

Fletcher, J. K., Parker, D. J., Hunt, K. M. R. ORCID: https://orcid.org/0000-0003-1480-3755, Vishwanathan, G. and Govindankutty, M. (2018) The interaction of Indian monsoon depressions with northwesterly mid-level dry intrusions. Monthly Weather Review, 146 (3). pp. 679-693. ISSN 0027-0644 doi: https://doi.org/10.1175/mwr-d-17-0188.1 Available at https://centaur.reading.ac.uk/75244/

To link to this article DOI: http://dx.doi.org/10.1175/mwr-d-17-0188.1

Publisher: American Meteorological Society

The DOI for this manuscript is doi: 10.1175/MWR-D-17-0188.1

The final published version of this manuscript will replace the preliminary version at the above DOI once it is available.

If you would like to cite this EOR in a separate work, please use the following full citation:

Fletcher, J., D. Parker, K. Hunt, G. Vishwanathan, and M. Govindankutty, 2018: The interaction of Indian monsoon depressions with northwesterly mid-level dry intrusions. Mon. Wea. Rev. doi:10.1175/MWR-D-17-0188.1, in press.

The interaction of Indian monsoon depressions with northwesterly mid-level dry intrusions

Jennifer K. Fletcher* and Douglas J. Parker

University of Leeds, Leeds, United Kingdom

Kieran M. R. Hunt

University of Reading, Reading, United Kingdom

Gokul Vishwanathan and Mrudula Govindankutty

CSIR-National Aerospace Laboratories, Bengaluru, India

**Corresponding author address:* School of Earth and Environment, University of Leeds, Leeds, LS6 9JT, United Kingdom.

E-mail: j.k.fletcher@leeds.ac.uk

ABSTRACT

Monsoon depressions (MDs) bring substantial monsoon rainfall to northern and central India. These events usually form over the Bay of Bengal and travel across northern India toward Pakistan. Using European Centre for Medium-Range Weather Forecasting Interim Reanalysis, an MD tracking algorithm, and an objective identification method, we find that about 40% of MDs interact with northerly intrusions of dry desert air masses as the MDs traverse the subcontinent. MD interactions with dry intrusions are often preceded by positive potential vorticity anomalies on the subtropical jet and low level anticyclonic anomalies over the north Arabian Sea. Dry intrusions nearly halve the precipitation rate in the southwest quadrant of MDs, where MDs rain the most. However, dry intrusions increase the rainfall rate near the MD center. Similarly, ascent is reduced west of the MD center and enhanced at the MD center, especially in the upper troposphere. The reduced ascent west of MD centers is likely attributable to changes in vertical shear reducing differential cyclonic vorticity advection. Dry intrusions slightly reduce MDs' propagation speed. For the mid-upper level vortex, this can be explained by anomalous westerlies reducing propagation by adiabatic advection. For the lower tropospheric vortex, it is likely that reduced diabatic generation of PV plays a role in slowing propagation, along with reduced adiabatic advection.

1. Introduction

The variability of northern India's summer monsoon includes frequent synoptic scale disturbances. Two of the most important of these are monsoon depressions and northwesterly dry intrusions. Monsoon depressions bring substantial monsoon rainfall to northern and central India. Dry intrusions from Pakistan and northwest India are thought to be essential to the pattern of the monsoon onset (Parker et al. 2016) and play a major role in monsoon breaks (Bhat 2006; Krishnamurti et al. 2010). In this paper we explore what happens when these two synoptic circulations interact.

Indian monsoon depressions (MDs) are synoptic-scale cyclonic disturbances which have average lifetimes of about 3 days but can last as long as a week (e.g., Hunt et al. 2016a). They usually make landfall on the east coast and occur about six times per season (June-September) (Sikka 1977). Sixty percent of MDs originate from the remnants of earlier disturbances that weaken over mainland Southeast Asia (Koteswaram and Bhaskara Rao 1963; Krishnamurti et al. 1977; Saha et al. 1981), with as many as a quarter being traceable to typhoons in the South China Sea (Saha et al. 1981). The structural features of MDs have been well described by previous authors (Godbole 1977; Sarker and Choudhary 1988; Prasad et al. 1990; Hurley and Boos 2015; Hunt et al. 2016a,b). The vortical structure of monsoon depressions is not axisymmetric due to the Himalayas, and they tend to rain disproportionately in their southwest quadrant (Mooley 1973; Hunt et al. 2016a).

Mechanisms for the typical westward propagation of MDs over the Indian subcontinent are not well understood. Rao and Rajamani (1970) and Sanders (1984) noted that the quasigeostrophic omega equation predicts ascent (and hence vortex stretching) west-southwest of the center, a result Chen et al. (2005) revisited using a composite streamfunction argument. Several authors (Goswami 1987; Sobel and Horinouchi 2000) have used Rossby wave analogies, but this has recently been contested by Boos et al. (2015), who took a vortex-centered view and presented evidence that MDs propagate by adiabatic advection of potential vorticity (PV), a result also supported by the analysis of Hunt and Parker (2016).

Prior to the monsoon onset, much of northern India is characterized by dry northerly and northwesterly winds in the lower troposphere and boundary layer (e.g., Parker et al. 2016). The erosion of this dry air mass by cumulus moistening has been proposed as an explanation for the characteristic northwestward progression of the monsoon isochrone (Parker et al. 2016). As the monsoon progresses, the low level winds transition to moist southwesterlies. However, intermittent pulses of dry northerly winds in the lower-mid troposphere (between about 700 and 400 hPa) occur throughout the monsoon season in northwestern India – we refer to these as dry intrusions. Krishnamurti et al. (2010) associated these dry intrusions with breaks in the monsoon and found that they are often preceded by a blocking high over the Arabian Peninsula.

In this paper, we explore the interaction of these major features of the north Indian monsoon. Figure 1 shows an example of such an interaction. The horizontal moisture gradient shown in Fig. 1d is dramatic and suggests some of the questions we address here. These questions include: How do dry intrusions affect the propagation and life cycle of monsoon depressions? What are the dynamical and thermodynamical effects? Are dry intrusions able to stir into the MD center or does the vorticity near the center block them?

The effect of dry intrusions may be important for MD rainfall in the Thar Desert region of northwestern India and Pakistan (location shown in Fig. 1a). In this region monsoon rainfall is more intermittent than in the rest of South Asia, because it is far from the moist monsoon flow and does not receive orographic enhancement of precipitation, as many other parts of northern India do. Substantial monsoon rainfall in these regions comes from monsoon depressions. While few MDs reach the Thar Desert region, those that do can be high impact events. We will show that the existence of dry intrusions is important for determining how much rainfall monsoon depressions produce over the more arid areas of northwestern India and Pakistan.

We explore the interaction between monsoon depressions and dry intrusions for the last thirty years of depressions. In Section 2 we describe the data and methods used, including an algorithm to objectively identify when these interactions occur. In Section 3 we compare the lifetimes, propagation speeds, and basic composite structure of MDs with and without dry intrusions. In Section 4 we examine the effect of dry intrusions over the life cycle of monsoon depressions. In Section 5 we examine the synoptic scale precursors to MD/dry intrusion interactions, including anomalies on the subtropical jet. In Section 6 we discuss some implications of this work, particularly for rainfall over the drier regions of the Thar Desert. We summarize and remark on possible future work in Section 7.

2. Data and methods

a. Atmospheric fields

We used the European Centre for Medium-Range Weather Forecasting Interim Reanalysis (Dee et al. 2011) for most atmospheric fields. This dataset was provided by the British Atmospheric Data Centre and is on a 0.7 degree horizontal grid for the years 1979-2015. This dataset was also used to create the monsoon depression tracks described in Section 2b. We used the temperature, winds, relative humidity, and potential vorticity on pressure levels as well as the mean sea level pressure and total column water in our calculations. We used the equation of Stull (2011) to compute wet bulb potential temperature from temperature and relative humidity on pressure levels.

For precipitation, we used the Tropical Rainfall Measuring Mission (TRMM) 3B42 gridded surface precipitation product for the years 1998-2015 (Huffman et al. 2007). Three hourly mean estimates are produced from TRMM's passive microwave radiometer and precipitation radar as well as from infrared radiometers, geostationary satellites' infrared brightness temperature, and rain gauges. The TRMM 3B42 data is on a 0.25 degree grid. Only data concurrent with the six-hourly ERA-Interim was used for precipitation associated with depressions, but all data was used for long term and monthly averages used in Section 6.

b. Monsoon depression tracking algorithm and dataset

Hunt et al. (2016a) developed an algorithm to identify and track Indian monsoon depressions on ERA-Interim data, corroborating the tracks with those published by the India Meteorological Department (IMD). The algorithm used here is essentially identical to that described in Hunt et al. (2016b), and when used on ERA-Interim, returns the dataset described by Hunt et al. (2016a). We provide a very brief outline below, and for full details the reader is encouraged to visit Chapter 2 of Hunt (2016). There are two parts to the algorithm: candidate identification and track linking.

To find potential candidates, we determine where in the data the IMD criteria of surface wind speed and surface pressure are satisfied. To do this with wind speed is simple, but surface pressure requires careful contour counting in the vicinity of the monsoon trough. Such candidates are then subject to a very low vorticity threshold to eliminate transient effects from orography, serving both to remove false positives and substantially speed up the track linking. The vorticity field is spectrally truncated to T42. The propagation constraints are: speed < 15 m s^{-1}, duration at least two days. The vorticity criterion is an area integral, about 10^{-5} s^{-1}. Track linking is carried out by a simple nearest-neighbor algorithm, subject to appropriate propagation constraints.

Applying this to ERA-Interim data recovers the 106-depression dataset described by Hunt et al. (2016a), so long as we apply their domain restriction: no MDs with genesis in the Arabian Sea, and all MDs must transition to (or originate over) land at some point during their lifetime. The algorithm outputs a timestamp, geographic coordinates, and heading for each (six-hourly) reanalysis timestep in each track.

The tracking algorithm only identifies MDs originating over the Bay of Bengal. It is likely that MDs originating over the Arabian Sea would commonly encounter dry intrusions. These would probably involve different large scale environments than the ones we found to be associated with MD/dry intrusion interactions in this work. However it would be interesting to include Arabian Sea depressions in future study of MD/dry intrusion interactions.

c. Objective identification of monsoon depression-dry intrusion interactions

Here we describe our algorithm for objective identification of interaction between MDs and dry intrusions. This algorithm was developed for this study and is only applied during instances when a monsoon depression was previously identified by the algorithm in Section 2b. Much of this algorithm's development was guided by visual examination of plots similar to those in Figure 1, over a range of pressure levels, for the 29 monsoon depression that occurred during the years 2000-2009.

First the algorithm calculates RH_{CTR}, the average relative humidity between 700 and 500 hPa over 3×3 gridpoints (roughly 150×150 km^2) centered on the MD center. 700-500 hPa was chosen because these are the heights where dry intrusions such as these have been studied before (e.g., Parker et al. 2016), and because we wanted to capture features that extended vertically over a significant depth. Then the algorithm calculates ΔRH, the difference between RH_{CTR} and the 700-500 hPa mean relative humidity of all gridpoints within ten degrees of MD center (in the western half only). It then searches for contiguous regions such that every gridpoint within the region has ΔRH greater than a specified threshold value. If at least one such contiguous region exceeds a threshold size, for two consecutive time steps, a dry intrusion interaction is diagnosed.

Below we will describe how we chose the threshold values used in the algorithm, but first we present an example. Figure 1 illustrates this process at various stages for a single MD. Panel a shows that the MD is far from the dry northwesterlies and no dry region is found within ten degrees of the MD center, which is indicated by the square black outline over the north Bay of Bengal. Twenty-four hours later, in Panel b, the dry intrusion has moved east and the MD has moved slightly west, so a small fraction of the area where ΔRH exceeds the threshold is within ten degrees of the MD. However, this area is not above the threshold size, and so no dry intrusion interaction is diagnosed.

Twelve hours later (Panel c), a large enough dry area is within ten degrees of the MD center that a dry intrusion interaction is diagnosed. In this example, all times prior to 2009-09-05-18Z are classified as pre-DI, and that time and all subsequent times are classified as post-DI. Panel d shows the interaction several days later, when the MD has propagated further west and swept the dry intrusion into the outer half of the MD circulation.

In order to choose the threshold values for ΔRH and the size of the dry region, we applied the algorithm to a range of thresholds. To do this, we calculated the frequency with which contiguous regions west of MDs of a specified size had ΔRH within a given bin. As in the identification algorithm, this ΔRH was applied to every gridpoint within the contiguous region, not just the mean. Figure 2 shows these distributions for several choices of specified region size. For all size choices, this distribution is skewed. It may be regarded as the sum of two distributions: a normal distribution representing the variation of mid-level relative humidity outside MDs and in the absence of dry intrusions, with a peak at $\Delta \text{RH} \simeq 20\%$; and a skewed distribution with a peak at about 50%, representing dry intrusions. The results suggest that a choice of threshold ΔRH of 40% or 50% and a threshold size of 40-60 gridpoints will capture the tail of the distribution.

We further tested the sensitivity of the algorithm to various parameters and assumptions, defining the sensitivity by checking how changes to those parameters and assumptions affected the number of MD-dry intrusion interactions identified and at what point in the lifespan of the MD a dry intrusion encounter was identified. We tested sensitivity to the following: the exclusion or inclusion of gridpoints with high orography; whether dry air masses are sought to the north as well as the west (so that only the southeast quadrant of the area around the MD was excluded from the search); the distance from MD center for which dry regions were searched; the threshold size of the dry air mass; and the threshold relative humidity difference between MD center and the dry air mass.

Some of these tests had only a small impact on the results. The parameters that the algorithm was sensitive to, and their effect on the number of identifications, is shown in Table 1. The final parameter choices were selected so as to eliminate false positives and minimize false negatives compared to events identified by the human eye for the subset of MDs occurring in the years 2000-2009. This human eye identification was done by examining plots of relative humidity and wet bulb potential temperature similar to those in Fig. 1.

We used this algorithm to group monsoon depressions in several ways. First, it categorises all MDs according to whether or not the algorithm detects and interaction with a dry intrusion (DI and noDI). Second, among the MDs that are classified as DI, we categorise them temporally into pre-DI and post-DI groups. Post-DI refers to all times including and after the first time that the algorithm detects MD interaction with a dry intrusion. Pre-DI refers to all times in the MD lifespan before this occurs.

d. Statistical significance tests

Differences in properties between DI and noDI were tested for statistical significance with a two-sided Student's t-test, with 95% confidence required. For tests involving data every ERA-Interim output time (e.g., those in Section 3c), the number of degrees of freedom was reduced from sample size N to N^* using the formula of Bretherton et al. (1999):

$$\frac{N^*}{N} = \frac{1-\exp\left(-\Delta t/T\right)}{1+\exp\left(-\Delta t/T\right)}, \tag{1}$$

with an output time step t of six hours and an autocorrelation e-folding time scale T of 24 hours for synoptic scale flow (Daoud et al. 2003).

3. The effect of dry intrusions on composite depressions

a. Number and tracks

Of 106 monsoon depressions identified between 1979 and 2014, 49 were identified as interacting with a dry intrusion. Figure 3 shows the effect of dry intrusions on MD tracks. The left panel shows the relative frequency of the locations of all MD centers in 3.0 degree latitude and longitude bins. The right panel shows the difference in track density between MDs with and without dry intrusions. Only locations with a statistically significant difference are plotted; significance is calculated as in Section 2d.

Tracks with dry intrusions show increased frequency in western and north-central India and a decreased frequency near the Bay of Bengal. This shows that MDs that propagate into western India are more likely than not to encounter a dry intrusion. We will discuss the effect of dry intrusions on MD rainfall in northwestern India and Pakistan in Section 6.

b. Lifetimes and propagation speed

As dicsussed in Section 1, MDs tend to make landfall at the north Bay of Bengal coast (Fig. 3). Some die out shortly thereafter or remain stationary in this area, while others propagate inland, generally to the northwest. We hypothesized that dry intrusions would particularly affect MD propagation into northwestern India. Of the 106 depressions in the database, 57 propagated west of 80°E. Table 2 shows the lifetime and propagation speeds of those 57 monsoon depressions subject to various conditions: 1) all, 2) noDI, 3) DI. The differences between lifetimes and propagation speeds in the subsets passed our statistical significance tests and were insensitive to the longitude threshold of 80°E.

Monsoon depressions with dry intrusions last about 10% longer than the average for all MDs and about 25% longer than those without dry intrusions. Possible reasons for this will be discussed in Section 3d. Dry intrusions also slow MD westward propagation, as Table 2 shows. MDs with dry intrusions propagate about 10% more slowly than those without dry intrusions. This will be discussed more in Section 3c.

c. Composite depressions

Figure 4 shows composites of horizontal winds and wet bulb potential temperature in monsoon depressions at 500 and 700 hPa. The origin of the composites is the center of the MDs. The left column shows composites of noDI depressions, the center shows DI depressions, and the right shows the difference. The effect of the composite dry intrusion is most evident to west and northwest of the depression center, with much lower wet bulb potential temperature at both pressure levels. At 500 hPa the effect of the dry intrusion is prominent even on the eastern side of the depression. At both levels it appears that the dry intrusion's impact reaches to within about 150 km of the center of the monsoon depression. The dry intrusion appears to encroach further south at 700 hPa than at 500 hPa. At 700 hPa the anomalous winds also appear more divergent outside the MD center.

Figure 5 shows the profound effect that dry intrusions have on precipitation in monsoon depressions. In the southwest quadrant of the depression, where the mean rainfall is greatest (left panel of Fig. 5), the precipitation is roughly halved (right panel of Fig. 5). We considered that this might be due to spatial sampling differences, since MDs with dry intrusions spend more time in central and western India than MDs without DIs do. If MDs tend to rain more in the humid monsoon trough region of northeastern peninsular India than in central and western India, then MDs with dry intrusions may rain less on average as an artifact of their average locations. As we will show in Section 6, MDs actually rain more in the west than in the east. It is therefore likely that the near halving of rainfall in the southwest quadrant of Fig. 5b is a direct effect of the dry intrusion. Intriguingly, dry intrusions are associated with an increase in rainfall near the MD center and to its north.

Figure 6 shows the effect of dry intrusions on the distribution of rainfall around MDs. Because rainfall maximizes to the southwest of MD centers, we sampled gridpoints within five degrees of the western half of MD center and within two degrees of the eastern half. The plots show the relative frequency of rainfall rates greater than 0.5 mm hr^{-1} (the 0-0.5 mm/h bin was included in the calculations but is not plotted). Fig. 6 shows that both categories of MDs have similar frequencies of low to moderate rain rates (below 10 mm hr^{-1}). MDs with dry intrusions have relatively lower frequencies of heavier rain rates compared to MDs without dry intrusions. Mid-level dry air can sometimes increase rates of extreme rainfall (e.g. Barnes and Sieckman 1984; Roca et al. 2005; Taylor et al. 2017), but for Indian monsoon depressions the effect of dry intrusions is to suppress extreme rainfall.

It is plausible that the reduced precipitation associated with dry intrusions is attributable to thermodynamic rather than dynamic effects. In other words, if two synoptic systems have the same circulation, but one has less moisture, that one will rain less. Figure 7 shows that this is not the scenario in Fig. 5, because dry intrusions have considerable dynamical effects in addition to reducing column moisture. Figure 7 shows vertical cross sections through the composites, along a line of constant latitude intersecting the MD center in the middle (the horizontal black line in Fig. 5a). As in Fig. 5b, all subplots of Fig. 7 show the difference between MDs with dry intrusions and those without.

Additionally, black contours in all panels of Fig. 7 show the potential temperature anomaly from the zonal mean within MDs with dry intrusions. These anomalies are calculated with respect to a mean from 20 degrees west to 20 degrees east of MD center. In the upper troposphere there is a warm anomaly to the west and a cold anomaly to the east. In the lower and mid-troposphere, the MD center is warm while the west is cold. The zero line begins at 400 hPa and 15 $^\circ$ west of MD center, dipping toward the surface and center of the MD, with air below and west of this line colder than average.

Figure 7a shows the composite mean zonal wind for all MDs. Comparing panels a and b, we see that the easterly shear is reduced by dry intrusions, primarily through a strong reduction in upper level easterlies but also through reduced low level westerlies.

A strong potential vorticity (PV) signature accompanies the dry intrusion (Fig. 7d). To the west of the MD center, dry intrusions are associated with a 1-2 PV Unit (10^{-6} m^2 s^{-1} K kg^{-1}) reduction in PV in the lower-mid troposphere. Near the MD center this reduction extends all the way to the surface. However, MDs with dry intrusions actually have higher PV at their center than those without, particularly in the upper troposphere. Hurley and Boos (2015) and Hunt et al. (2016a) found a PV maximum in MD centers at 500 hPa. The PV anomaly here suggests that the vortices of MDs with dry intrusions are deeper both geometrically and in terms of strength. The MD center has greater vorticity, stronger ascent, and more rainfall (the ascent difference is only statistically significant at about 850 hPa and between 200-500 hPa).

Outside the MD center, the PV is lower than in MDs without dry intrusions. The tongue of low PV dipping toward the surface from the west is likely a combination of advection of low PV from the west and reduction in diabatic PV generation west of MD center, consistent with the reduction in precipitation. The PV increase near the center may be diabatically generated in the lower troposphere; we also found evidence that the centers of MDs with dry intrusions are slightly more closed off to stirring from the outside; this may preserve the high PV near the center. We will discuss this further in Section 3d.

PV is reduced to the east of the MD center as well as to its west, and Figure 8 also shows that it is reduced to the south. It is possible that dry intrusions reduce the size of MDs, which may be related to the strengthening of the vorticity at MD center.

The circulation associated with the PV anomalies is indicated by schematic arrows into and out of the page in Fig.7d. The meridional wind anomalies (Fig. 7c) are consistent with those expected from the combined effect of low-high-low PV anomalies in a west-east cross section. The vorticity-induced circulation differences would partially offset the climatological northwestward trajectory of MDs. The low PV to the west induces a relatively anticyclonic flow around it, while the high PV at the center induces a relatively cyclonic circulation around the MD center. Between these locations of low and high PV, the induced circulations add to produce northerly flow to the immediate west of the MD center in the lower troposphere. PV anomalies to the east would also induce southerly flow east of the MD center, especially in the upper troposphere.

In Fig. 7e, we see increases in pressure velocity (reduced ascent) to the west of the MD center, extending to near the tropopause. The increase in rainfall near the MD center is accompanied by increased ascent there between 900 and 400 hPa.

The effect of dry intrusions on ascent might be understood partially in terms of the quasi-geostrophic (QG) omega equation for adiabatic, frictionless flow (e.g. Trenberth 1978; Boos et al. 2015), focusing on terms most relevant for Fig. 7:

$$L\omega \sim -2f_0 \frac{\partial \mathbf{u}_g}{\partial p} \cdot \nabla \zeta_g, \tag{2}$$

where L is a Laplacian operator, ω is the pressure velocity, f_0 is the f-plane approximation of the Coriolis parameter, $\mathbf{u}_g$ and ζ_g are the geostrophic wind vectors and relative vorticity.

Boos et al. (2015) showed that the full QG forcing (which includes terms not shown in Eqn. 2) qualitatively predicted ascent to the southwest of the MD center and descent to its northeast. All else being equal, the change in zonal wind shear shown in Fig. 7b will reduce the differential advection of PV with height, reducing ascent west of the MD centre and reducing descent to its east. Conversely, there is a slight increase in westerly shear at the MD center between 850 hPa and 500 hPa, which could force the increased ascent in that region, where the positive vorticity anomaly is also slightly west of the MD center. It is also possible that convective responses to the enhanced temperature gradient and mid-level dry layer are driving the increased ascent near the MD center.

Figure 7 suggests the cause of the reduction in MD propagation speed with dry intrusions (Table 2). Boos et al. (2015) suggested that MDs propagate by adiabatic advection of PV. They primarily identified this mechanism for the 500 hPa PV maximum observed at MD centers, which is advected westward by the wind at that height. They also identified a 700 hPa PV maximum, and argued that it propagated northwestward through a combination of horizontal advection to the north-northwest and diabatic PV tendencies to the southwest.

The dry intrusion is associated with anomalous westerlies in the upper troposphere, slowing the westward advection of the 500 hPa maximum. The dry intrusion directly reduces positive diabatic PV tendencies in the lower troposphere to the southwest of MD centers through its suppression of convection and rainfall in that location. Furthermore, the anticyclonic PV anomaly in the lower troposphere west of the MD center induces a circulation that would advect the MD vortex southward. We suggest that this combination of mechanisms slows MD propagation in the presence of dry intrusions.

Figure 7f shows the composite difference in potential temperature. In most of the troposphere the composite potential temperature is lower in depressions that encounter dry intrusions, especially west of the MD center where convection and precipitation are suppressed (Figs 7e and 5b). However, it is warmer in the upper troposphere. Some of the upper troposphere anomaly has the same horizontal structure as the PV anomaly in the same location, suggesting a lowering of the tropopause.

Figure 8 shows the meridional cross section of PV through the MD center (i.e., the vertical line in Fig. 5a) and the composite difference of 100 hPa PV. In the meridional cross section, the lower tropospheric differences in the north are not statistically significant and occur at pressure levels higher than mean surface pressure north of the median locations of MD centers. The biggest difference is between 300 and 100 hPa, where MDs with dry intrusions have much higher PV. In this same region is a large (5-20 K) potential temperature anomaly (not shown), suggesting a lowering of the tropopause in this region. The PV anomaly is also seen in the 100 hPa cross section, where a very large positive PV anomaly extends over most of the northern half of the cross section. As we will show in Section 5, this is evidence for extratropical precursors to the dry intrusion.

d. How easily can the dry intrusion stir into the MD?

At this point it is still unclear how effective the dry intrusion is at mixing in dry desert air with the monsoon depression – how much stirring is really happening between these two air masses? To address this we use the Okubo-Weiss parameter (Okubo 1970; Weiss 1991), which has been used in ocean dynamics to identify eddies (e.g., Chang and Oey 2014). For the horizontal flow, the Okubo-Weiss parameter Δ is defined as:

$$\Delta = \left(\frac{\partial u}{\partial x} - \frac{\partial v}{\partial y}\right)^2 + \left(\frac{\partial v}{\partial x} + \frac{\partial u}{\partial y}\right)^2 - \left(\frac{\partial v}{\partial x} - \frac{\partial u}{\partial y}\right)^2. \quad (3)$$

The three parenthesized terms on the right hand side of Equation 3 are the stretching deformation, the shearing deformation, and the vorticity, respectively. If the third term is larger than the sum of the first two, $\Delta < 0$ and the flow is eddy-like. This inhibits stirring with external air masses. If $\Delta > 0$, the flow is subject to large scale mixing. We expect the dry intrusion to have a greater effect on the monsoon depression in regions where $\Delta > 0$.

Figure 9 shows the composite average value of this parameter at 700 hPa for all MDs as well as the difference between DI and noDI cases. The pattern at 500 hPa (not shown) is similar but weaker in magnitude. For all MDs the sign of Δ is mostly positive, with a negative core near and slightly southeast of the MD center. This negative core is slightly larger in magnitude and horizontal scale for MDs that do encounter dry intrusions, and extends further west. This is consistent with the higher PV seen near the core of these MDs. The enhanced vorticity somewhat shields the MD center from the dry intrusion. The most likely region for remote air to mix into the MD center is to the north and northeast, where Δ is reduced in MDs with dry intrusions. In summary, while the southeast quadrant of MDs, which produce the heaviest rainfall on average, are strongly affected by dry intrusions, the MD center is mostly insulated from them.

4. The effect of dry intrusions on MD life cycle

Figures 10 and 11 show the development of the composite monsoon depression before and during interaction with a dry intrusion. The times shown in each panel indicate the number of hours before or after the MD was first identified to encounter a dry intrusion. In other words, $t = 0$ is the first time the criteria in Section 2c were satisfied. Only pre-identified MDs were included in the composite at each time lead/lag. Because MDs have different life spans, not all members of the composite at $t = 0$ hours were included at earlier and later lead/lags.

Figure 10 shows total column water (TCW). The arc of very low water content in the northern sector of all plots indicates the typical location of high orography with respect to the MD. As the MDs propagate westward (the later panels), the high orography of northwestern Pakistan and Afghanistan comes into view; the very low TCW in the upper left is more associated with topography than with the dry intrusion. However, closer to the composite MD center we see a steady drop in TCW to the west of the MD. As early as twelve hours after the interaction is identified (Fig 10d), substantial drying out is seen to the south of the composite MD as well as to the west, as the MD incorporates the dry intrusion into its circulation. By 24 hours, the effect of the dry intrusion is seen throughout the MD, including near its center, although the effect is most prominent to the west and south. In particular the very high TCW to the southwest of MD center in Panel a is severely eroded by Panel f.

Figure 11 shows the development of potential vorticity at 700 hPa. Figure 7d shows that this is not the height where the dry intrusion most affects PV – that occurs lower than 700 hPa. However as Hurley and Boos (2015) and Hunt et al. (2016a) have shown, 700 hPa is a height where potential vorticity peaks in monsoon depressions. Prior to the dry intrusion, a stream of high PV seems to be advected from the Himalayan foothills. This stream is cut off by low PV associated with the dry intrusion. The dry intrusion source air is typically the deserts of Pakistan and Afghanistan; this is a region of climatologically low PV (Fig. 12). There is anticyclonic PV advection from the west toward the edge of the MD circulation prior to the interaction. The ongoing reduction in PV after the interaction occurs is likely a combination of anticyclonic PV advection from the dry intrusion and the reduction of midtropospheric diabatic warming due to suppressed convection west of the MD center. While quantitative treatment of PV tendency terms is not possible with this data, Fig.11 suggests that it is more the latter than the former, as the flow is mostly parallel with PV contours.

5. Synoptic precursors to dry intrusion

Figure 13 shows the wind and potential vorticity anomalies from climatology twenty four hours before an interaction between a monsoon depression and a dry intrusion. Only statistically significant anomalies are shown.

The upper tropospheric circulation anomalies associated with a dry intrusion are largest in the vicinity of the subtropical jet, where a cyclonic PV anomaly induces anomalous northerlies over Central and South Asia. Preliminary work (not shown) indicates that MDs with dry intrusions are much more likely to coincide with what the Indian Meteorological Department calls eastward moving systems – cyclonic anomalies in the subtropical jet over South Asia. The interactions between MDs, dry intrusions, and the extratropics will be explored more in future work.

In the lower troposphere (700-500 hPa, right panel), the winds and PV show anomalous anticyclonic circulation over the north Arabian Sea. Blocking highs over the Arabian peninsula have already been associated with dry intrusions from the northwest, often preceding monsoon breaks (Krishnamurti et al. 2010).

6. Implications for northwestern India and Pakistan rainfall

Figure 14 highlights the effect of monsoon depressions on rainfall across northern India. The solid lines show the mean rainfall within eight degrees of MD centers, averaged over land points only from 20-30 N. In northeast India, near the head of the Bay of Bengal, the mean rainfall associated with MDs is comparable to the mean daily rainfall during the monsoon (dashed line), suggesting that MDs are not major contributors to seasonal rainfall anomalies in that region. Interestingly, in this region DI MDs produce more rainfall than non-DI. This is likely because for this latitude and longitude band, we are disproportionately sampling areas to the north of the MD centre, where dry intrusions are associated with an increase in rainfall (Fig. 5). Moving to the west, the mean monsoon season rainfall decreases while the mean rainfall associated with MDs largely increases. This increases the potential for MDs to bring substantial rainfall anomalies. However, west of about 77°E, MDs with dry intrusions produce considerably less rain.

The black line in Fig. 14 shows rainfall for all MDs, and thus we can infer that locations where it is very close to the DI or noDI line are regions where most MD rainfall lies in that respective category. This tells us that while MDs are more likely than not to have dry intrusions when they are very far west (Fig. 3), the ~1000 km horizontal scale of MDs means that even systems centered over central India, with no dry intrusion, can produce strong rainfall over western India and Pakistan. However, when these systems encounter dry intrusions, the drop in rainfall to their west can preclude this.

7. Summary and conclusion

We applied an objective identification algorithm to 106 Indian monsoon depressions over the ERA-Interim period and identified 49 which encounter an intrusion of dry mid-tropospheric air, mostly from the northwest deserts. These dry intrusions are associated with cyclonic PV anomalies on the subtropical jet to the northwest and low level anticyclonic circulation over the north Arabian Sea. They advect air masses with climatologically low PV and humidity southeastward toward central India. The impact of dry intrusions on MDs is summarized in Figure 15. When a monsoon depression encounters a dry intrusion, it sweeps the dry air mass into its own circulation.

The effect of dry intrusions includes:

- A near near 50% reduction of surface precipitation in the southwest quadrant of the depression, where precipitation is greatest in MDs generally;
- A 25% increase in MD lifetime compared to MDs with no dry intrusion;
- A 10% reduction in propagation speed;
- A reduction in potential vorticity and vertical ascent, as well as a weakening of shear in the zonal wind, west of the depression center;
- An increase in potential vorticity and rainfall, near and slightly east of the MD center, particularly in the upper troposphere.

Anomalous westerlies are expected to slow MD propagation by adiabatic advection as proposed by (Boos et al. 2015), while suppression of convection would reduce the positive PV tendency in the lower troposphere to the southeast of the MD center, reducing the propagation of the lower tropospheric vortex. These mechanisms are consistent with the slowing of MD propagation observed when it encounters a dry intrusion. Changes in shear are also consistent with the observed reduction in ascent and rainfall west of MD center, as such changes reduce the differential vorticity advection term in the QG omega equation.

This work has opened many new questions. What are the sources and sinks of potential vorticity to account for the differences seen? What is the convective scale response to the changes induced by the dry intrusion, and how does that response feed back on mesoscale and synoptic scale circulations? Data resolving mesoscale circulations and deep convection may be needed to adequately address this question. We also plan to investigate the effect of dry intrusions on convective organisation in future work.

In July 2016, the combined United Kingdom National Environmental Research Council and Indian Ministry of Earth Sciences project entitled Interaction of Convective Organization and Monsoon Precipitation, Atmosphere, Surface, and Sea (INCOMPASS) flew the UK atmospheric research aircraft BAe146 through a monsoon depression. This depression encountered a dry intrusion and substantial horizontal gradients in moisture were observed. In upcoming work those involved in the INCOMPASS campaign will present analysis of aircraft data from this depression as well as a high resolution convection-permitting simulation of the same case. With this we will be able to examine the dynamics of this interaction more closely and address the questions above.

Acknowledgments. This research was supported by UK National Environment Research Council grant NE/L013843/1. Douglas Parker is also supported by a Royal Society Wolfson Research Merit Award. We thank William Boos, Michael Reeder, Andrew Turner, and two anonymous reviewers for insightful comments and suggestions.

References

Barnes, G., and K. Sieckman, 1984: The environment of fast-and slow-moving tropical mesoscale convective cloud lines. *Mon. Wea. Rev.*, **112 (9)**, 1782–1794.

Bhat, G. S., 2006: The indian drought of 2002a sub-seasonal phenomenon? *Quarterly Journal of the Royal Meteorological Society*, **132 (621)**, 2583–2602.

Boos, W. R., J. V. Hurley, and V. S. Murthy, 2015: Adiabatic westward drift of Indian monsoon depressions. *Quart. J. Roy. Meteor. Soc.*, **141 (689)**, 1035–1048, doi:10.1002/qj.2454, URL http://dx.doi.org/10.1002/qj.2454.

Bretherton, C. S., M. Widmann, V. P. Dymnikov, J. M. Wallace, and I. Bladé, 1999: The effective number of spatial degrees of freedom of a time-varying field. *J. Climate*, **12 (7)**, 1990–2009.

Chang, Y.-L., and L.-Y. Oey, 2014: Analysis of stcc eddies using the okubo–weiss parameter on model and satellite data. *Ocean Dynamics*, **64 (2)**, 259–271.

Chen, T.-C., J.-H. Yoon, and S.-Y. Wang, 2005: Westward propagation of the Indian monsoon depression. *Tellus*, **57A**, 758–769, doi:10.1111/j.1600-0870.2005.00140.x, URL http://dx.doi.org/10.1111/j.1600-0870.2005.00140.x.

Daoud, W. Z., J. D. Kahl, and J. K. Ghorai, 2003: On the synoptic-scale Lagrangian autocorrelation function. *J. Appl. Meteor.*, **42 (2)**, 318–324.

Dee, D. P., and Coauthors, 2011: The ERA-Interim reanalysis: configuration and performance of the data assimilation system. *Quart. J. Roy. Meteor. Soc.*, **137 (656)**, 553–597, doi:10.1002/qj.828, URL http://dx.doi.org/10.1002/qj.828.

Godbole, R. V., 1977: The composite structure of the monsoon depression. *Tellus*, **29**, 25–40, doi:10.1111/j.2153-3490.1977.tb00706.x, URL http://dx.doi.org/10.1111/j.2153-3490.1977.tb00706.x.

Goswami, B. N., 1987: A mechanism for the west-north-west movement of monsoon depressions. *Nature*, **326**, 376–378, doi:10.1038/326376a0, URL http://dx.doi.org/10.1038/326376a0.

Huffman, G. J., and Coauthors, 2007: The trmm multisatellite precipitation analysis (tmpa): Quasi-global, multiyear, combined-sensor precipitation estimates at fine scales. *J. Hydrometeor.*, **8 (1)**, 38–55.

Hunt, K. M., and D. J. Parker, 2016: The movement of indian monsoon depressions by interaction with image vortices near the himalayan wall. *Quarterly Journal of the Royal Meteorological Society*, **142 (698)**, 2224–2229.

Hunt, K. M., A. G. Turner, P. M. Inness, D. E. Parker, and R. C. Levine, 2016a: On the structure and dynamics of Indian monsoon depressions. *Mon. Wea. Rev.*, **144 (9)**, 3391–3416.

Hunt, K. M., A. G. Turner, and D. E. Parker, 2016b: The spatiotemporal structure of precipitation in Indian monsoon depressions. *Quart. J. Roy. Meteor. Soc.*

Hunt, K. M. R., 2016: On the behaviour of tropical depressions and their interaction with the Indian monsoon trough region. Ph.D. thesis, University of Reading.

Hurley, J. V., and W. R. Boos, 2015: A global climatology of monsoon low-pressure systems. *Quart. J. Roy. Meteor. Soc.*, **141 (689)**, 1049–1064, doi:10.1002/qj.2447, URL http://dx.doi.org/10.1002/qj.2447.

Koteswaram, P., and N. S. Bhaskara Rao, 1963: Formation and structure of indian summer monsoon depressions. *Aust. Meteor. Mag.*, **41**, 2–75.

Krishnamurti, T., A. Thomas, A. Simon, and V. Kumar, 2010: Desert air incursions, an overlooked aspect, for the dry spells of the Indian summer monsoon. *J. Atmos. Sci.*, **67 (10)**, 3423–3441.

Krishnamurti, T. N., J. Molinari, H. Pan, and V. Wong, 1977: Downstream amplification and formation on monsoon disturbances. *Mon. Wea. Rev.*, **105**, 1281–1297.

Mooley, D. A., 1973: Some Aspects of Indian Monsoon Depressions and the Associated Rainfall. *Mon. Wea. Rev.*, **101 (3)**, 271–280, doi:10.1175/1520-0493(1973)101⟨0271:SAOIMD⟩2.3.CO;2.

Okubo, A., 1970: Horizontal dispersion of floatable particles in the vicinity of velocity singularities such as convergences. *Deep sea research and oceanographic abstracts*, Elsevier, Vol. 17, 445–454.

Parker, D. J., P. Willetts, C. Birch, A. G. Turner, J. H. Marsham, C. M. Taylor, S. Kolusu, and G. M. Martin, 2016: The interaction of moist convection and mid-level dry air in the advance of the onset of the Indian monsoon. *Quart. J. Roy. Meteor. Soc.*

Prasad, K., S. R. Kalsi, and R. K. Datta, 1990: On some aspects of wind and cloud structure of monsoon depressions. *Mausam*, **41**, 365–370.

Rao, K., and S. Rajamani, 1970: Diagnostic study of a monsoon depression by geostrophic baroclinic model. **21**, 187–194.

Roca, R., J.-P. Lafore, C. Piriou, and J.-L. Redelsperger, 2005: Extratropical dry-air intrusions into the West African monsoon midtroposphere: An important factor for the convective activity over the Sahel. *J. Atmos. Sci.*, **62 (2)**, 390–407.

Saha, K., F. Sanders, and J. Shukla, 1981: Westward propagating predecessors of monsoon depressions. *Mon. Wea. Rev.*, **109 (2)**, 330–343, doi:10.1175/1520-0493(1981)109⟨0330:WPPOMD⟩2.0.CO;2.

Sanders, F., 1984: Quasi-geostrophic diagnosis of the monsoon depression of 58 July 1979. *J. Atmos. Sci.*, **41**, 538–552, doi:10.1175/1520-0469(1984)041⟨0538:QGDOTM⟩2.0.CO;2, URL http://dx.doi.org/10.1175/1520-0469(1984)041⟨0538:QGDOTM⟩2.0.CO;2.

Sarker, R. P., and A. Choudhary, 1988: A diagnostic study of monsoon depressions. *Mausam*, **39**, 9–18.

Sikka, D. R., 1977: Some aspects of the life history, structure and movement of monsoon depressions. *Pure Appl. Geophys.*, **115**, 1501–1529, doi:10.1007/BF00874421, URL http://dx.doi.org/10.1007/BF00874421.

Sobel, A. H., and T. Horinouchi, 2000: On the dynamics of easterly waves, monsoon depressions, and tropical depression type disturbances. *J. Meteor. Soc. Japan*, **78 (2)**, 167–173.

Stull, R., 2011: Wet-bulb temperature from relative humidity and air temperature. *J. Appl. Meteor. Climatol.*, **50 (11)**, 2267–2269.

Taylor, C. M., and Coauthors, 2017: Frequency of extreme Sahelian storms tripled since 1982 in satellite observations. *Nature*, **544 (7651)**, 475–478.

Trenberth, K. E., 1978: On the interpretation of the diagnostic quasi-geostrophic omega equation. *Mon. Wea. Rev.*, **106 (1)**, 131–137.

Weiss, J., 1991: The dynamics of enstrophy transfer in two-dimensional hydrodynamics. *Physica D: Nonlinear Phenomena*, **48 (2-3)**, 273–294.

LIST OF TABLES

TABLE 1. The effect of the threshold dry air mass size (in gridpoints, first column); threshold ΔRH; and distance from MD center for which a dry intrusion is searched (degrees, third column) on MD/dry intrusion identification. Fourth column gives the number of MDs identified to encounter a dry intrusion. Final column shows the average time difference in which a dry intrusion interaction is first identified compared to the control (first data row), e.g., changing the required air mass size from 50 to 60 gridpoints delays the identification by an average of four hours.

dry air mass size	Δ RH threshold	Distance threshold	Num. DI events	Start time difference
50 gridpoints	40%	10°	49	NA
60 gridpoints	40%	10°	44	4 h
50 gridpoints	50%	10°	32	16 h
50 gridpoints	40%	8°	29	12 h

TABLE 2. Lifetime and propagation speed of Indian monsoon depressions that propagate west of 80°E: all MDs, MDs with no dry intrusions, and MDs with dry intrusions. All differences between DI and noDI were found to be significant (see Section 2d, number of degrees of freedom = number of events).

MD category	Number of events	lifetime (days)	prop. speed (m s^{-1})
All	47	4.3 ± 1.6	3.3 ± 0.9
noDI	21	3.8 ± 0.8	3.5 ± 0.9
DI	26	4.8 ± 2.0	3.1 ± 0.9

LIST OF FIGURES

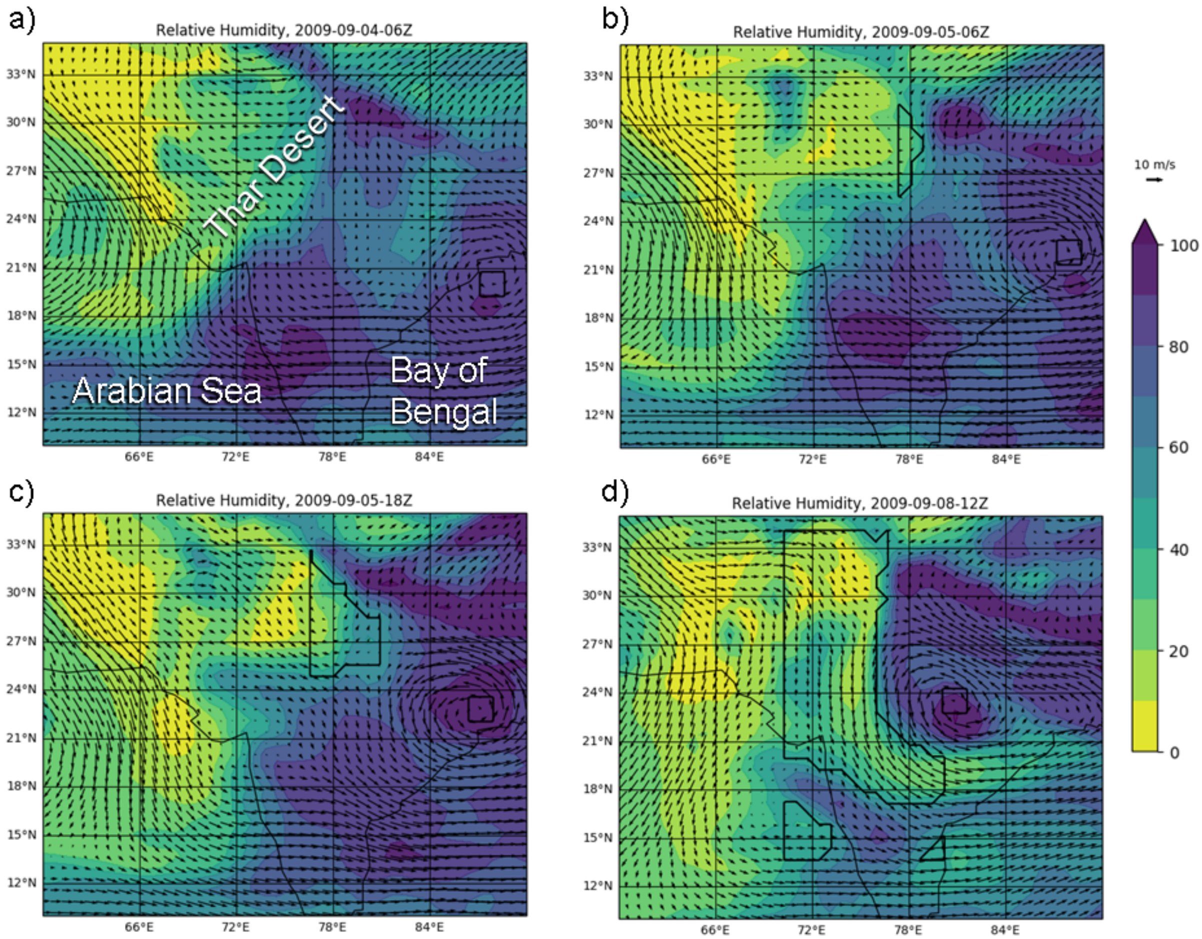

FIG. 1. Relative humidity and horizontal winds on the 700 hPa pressure surface from ERA-Interim during a monsoon depression with a dry intrusion on 8 September 2009. Black box indicates the location of MD center plus or minus one gridpoint in latitude and longitude. Other black-outlined shapes are dry regions within ten degrees of MD center, described in Section 2c.

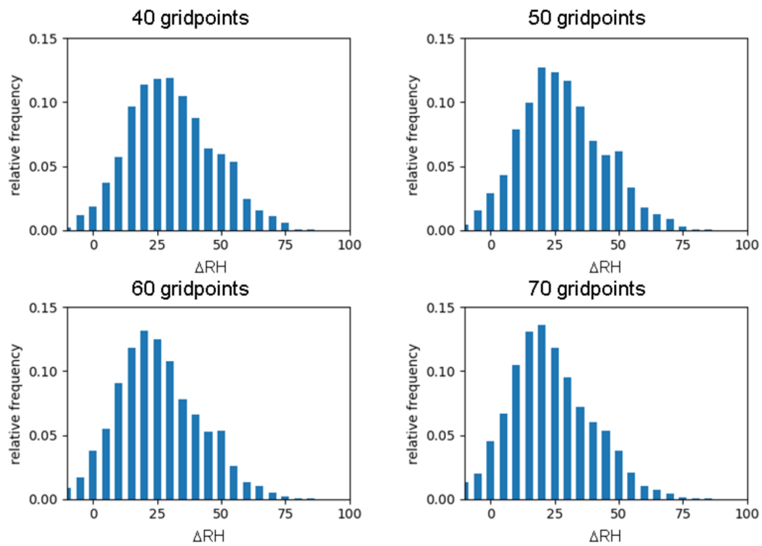

FIG. 2. Distribution of the maximum relative humidity contrast (700-500 hPa vertical mean) between monsoon depression centers and a region to the west of varying minimum sizes.

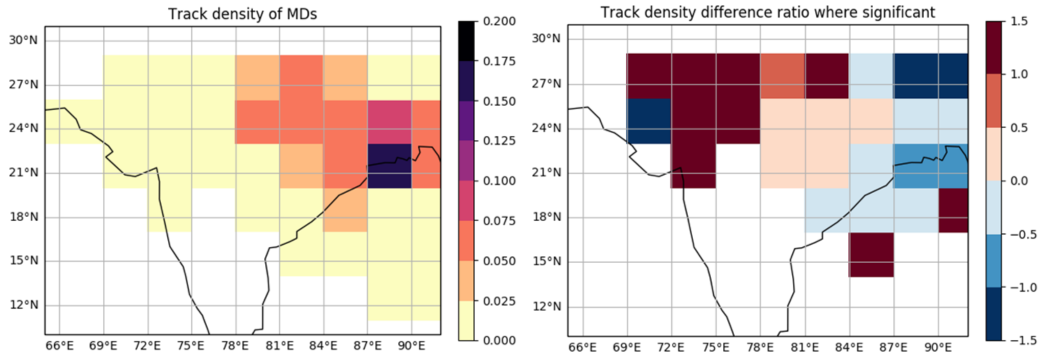

FIG. 3. Track density of monsoon depressions. Left: all MDs. Right: difference between MDs with and without dry intrusions where statistically significant (blue indicates locations with higher frequency of MDs without dry intrusions; red indicates locations with higher frequency of MDs with them).

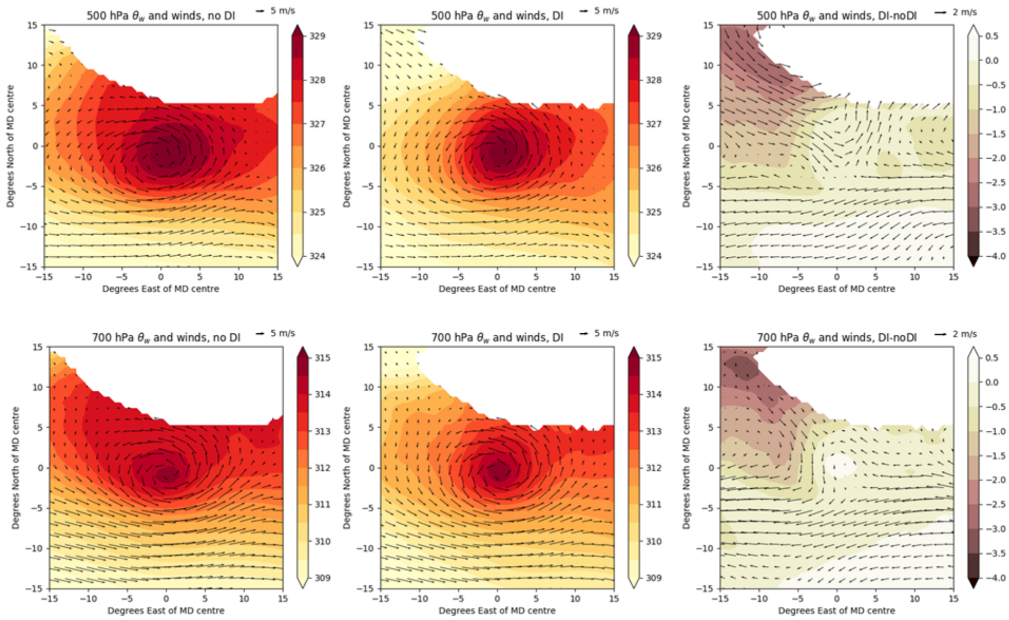

FIG. 4. Composites of 500 hPa (top) and 700 hPa (bottom) wet bulb potential temperature [K] and horizontal winds for monsoon depressions without (left, noDI) and with (center, DI) dry intrusions. Right column shows the difference (DI composites minus noDI composites). Masked areas are locations where high orography occurs frequently within the composites. Composites are for the full MD lifecycle. Note different color scales between top and bottom rows and different wind vector scales between mean composites and differences.

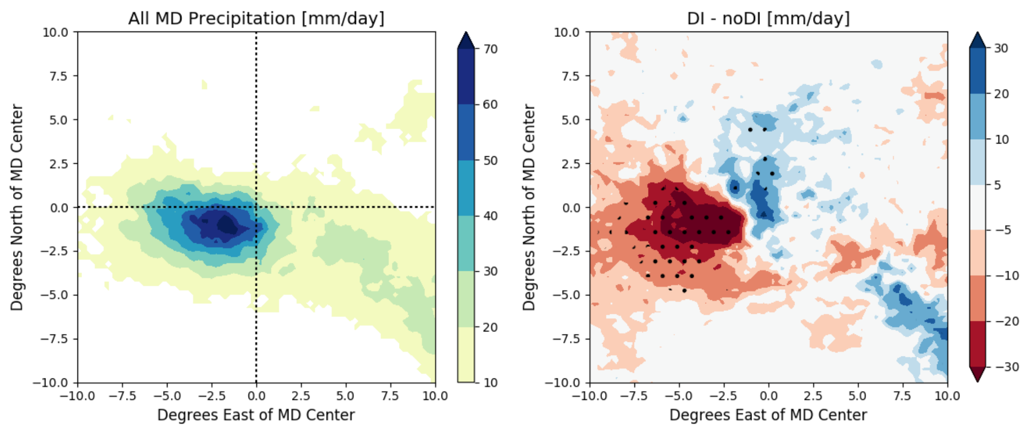

FIG. 5. Precipitation in all composite MDs (left), and precipitation difference between MDs with and without dry intrusions (right). Dots on the right panel indicate statistical significance, calculated as described in Section 2d (the assumed autocorrelation time scale for precipitation is 12 hours rather than 24). Black dotted lines on the left panel indicate locations of vertical cross sections presented in later figures. Composites are for the full MD lifecycle.

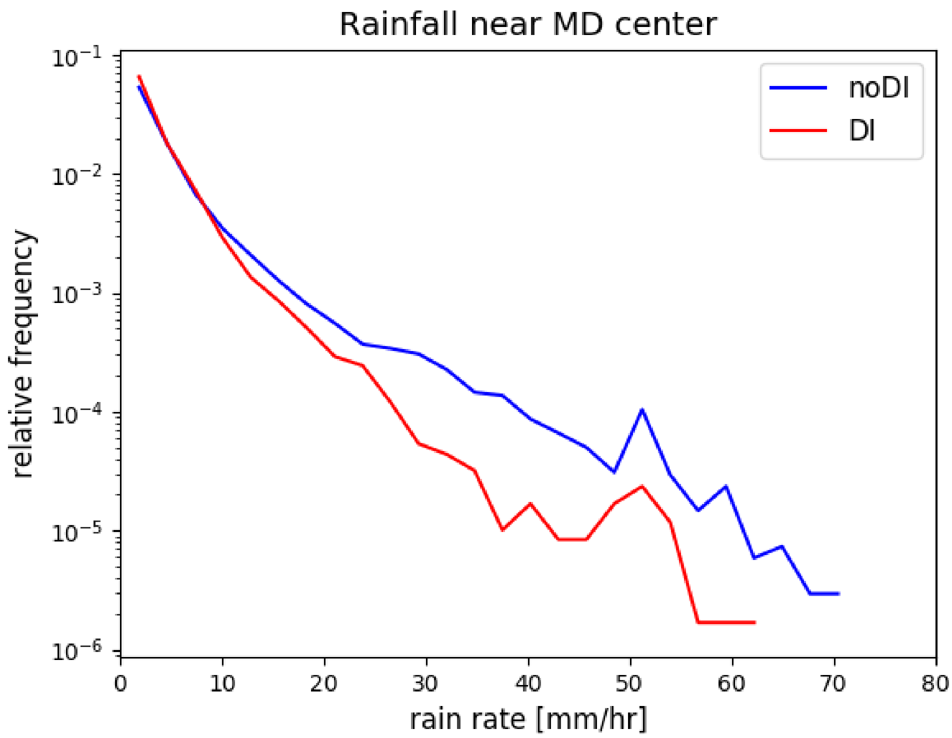

FIG. 6. Relative frequency of rain rates exceeding 0.5 mm hr^{-1} for MDs with and without dry intrusions (red and blue lines, respectively).

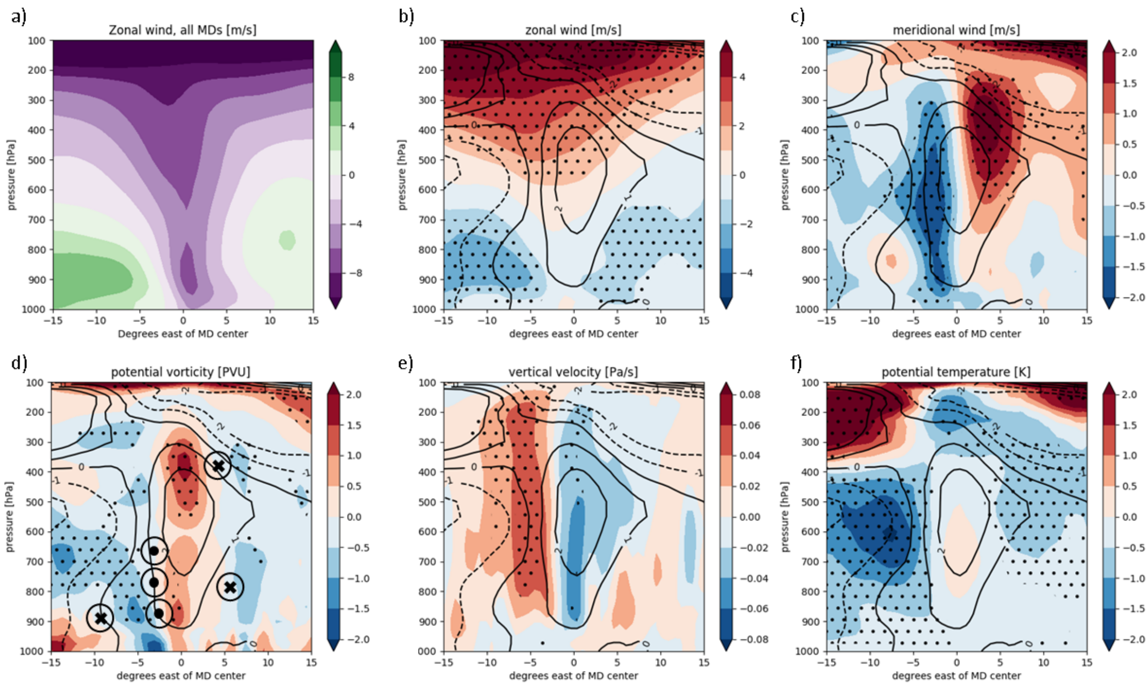

FIG. 7. a) Zonal wind in all MDs in a vertical, west to east cross section through the center of composites as indicated in Fig. 5a. b-f) Difference between composites of monsoon depressions with and without dry intrusions (DI-noDI). Black contours indicate the potential temperature anomaly from the zonal mean within MDs with dry intrusions. Dots indicate statistical significance at 95% confidence, calculated as in Section 2d. In Panel d, encircled dots and crosses indicate meridional wind anomalies implied by circulation around the PV anomalies, and one PVU = 1.0×10^{-6} m^2 s^{-1} K kg^{-1}. Composites are for the full MD lifecycle.

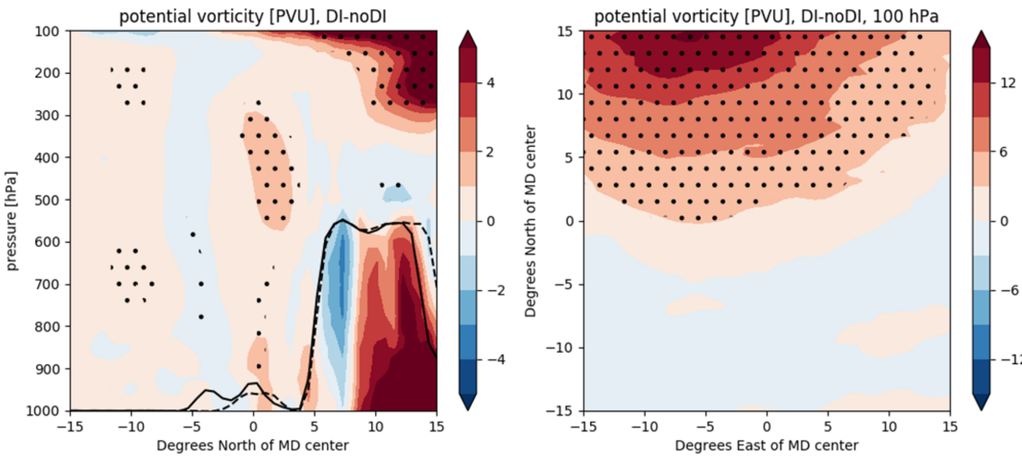

FIG. 8. Left: vertical, south-north cross section of the difference in composite PV between MDs with and without dry intrusions. Dots indicate statistical significance. Solid (dashed) black lines indicate orography north and south of the median location of MDs with (without) dry intrusions. The location of the cross section is indicated by the vertical line in Fig. 5. Right: horizontal composite of PV at 100 hPa. Units are PVU in both panels, and composites are over full MD lifetimes.

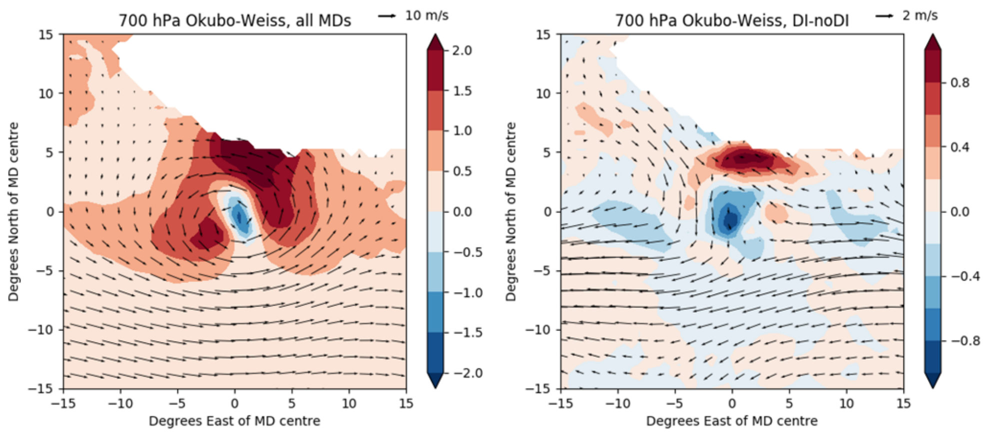

FIG. 9. Composites of the Okubo-Weiss parameter (Eq. 3) in (left) all depressions, and (right) DI-noDI. Units are 10^{-9} s^{-1}, and composites are over full MD lifetimes.

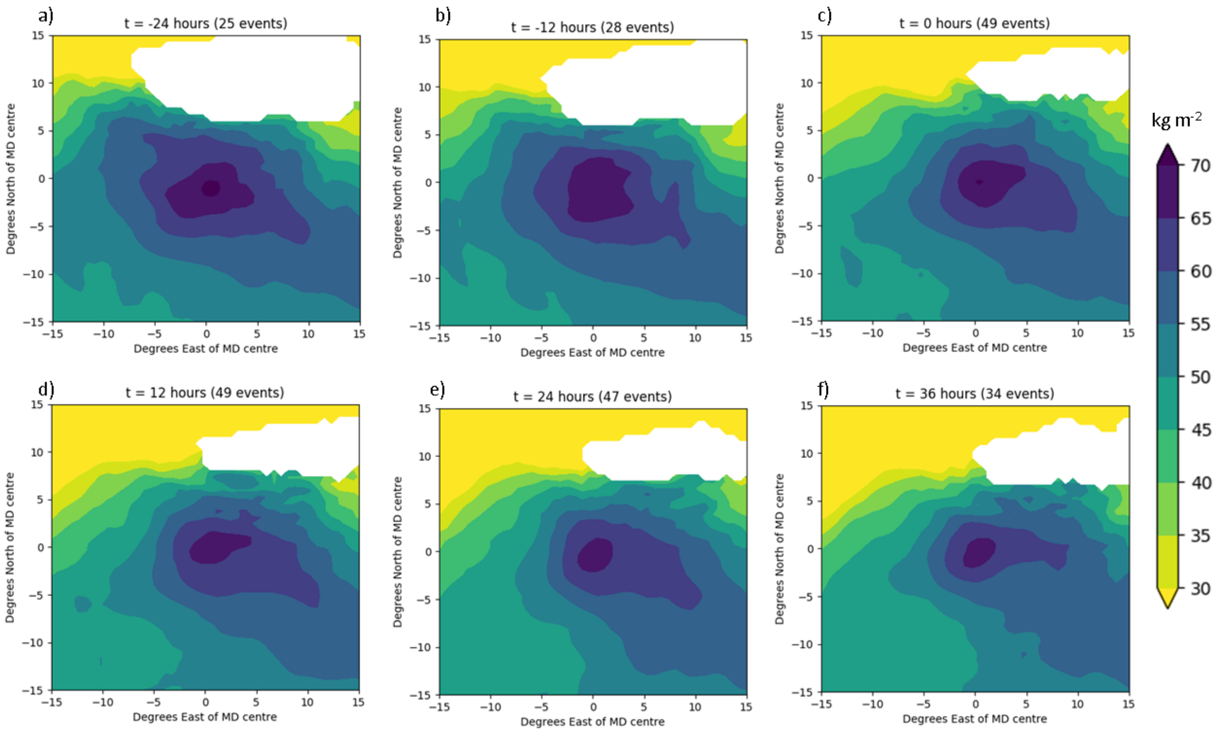

FIG. 10. Composites of total column water [kg m^{-2}] centered on MDs with dry intrusions leading up to and after the interaction with the dry intrusion. t indicates the number of hours since the beginning of interaction with a dry intrusion. Locations where orography is below 3000 m for fewer than ten composite members are masked.

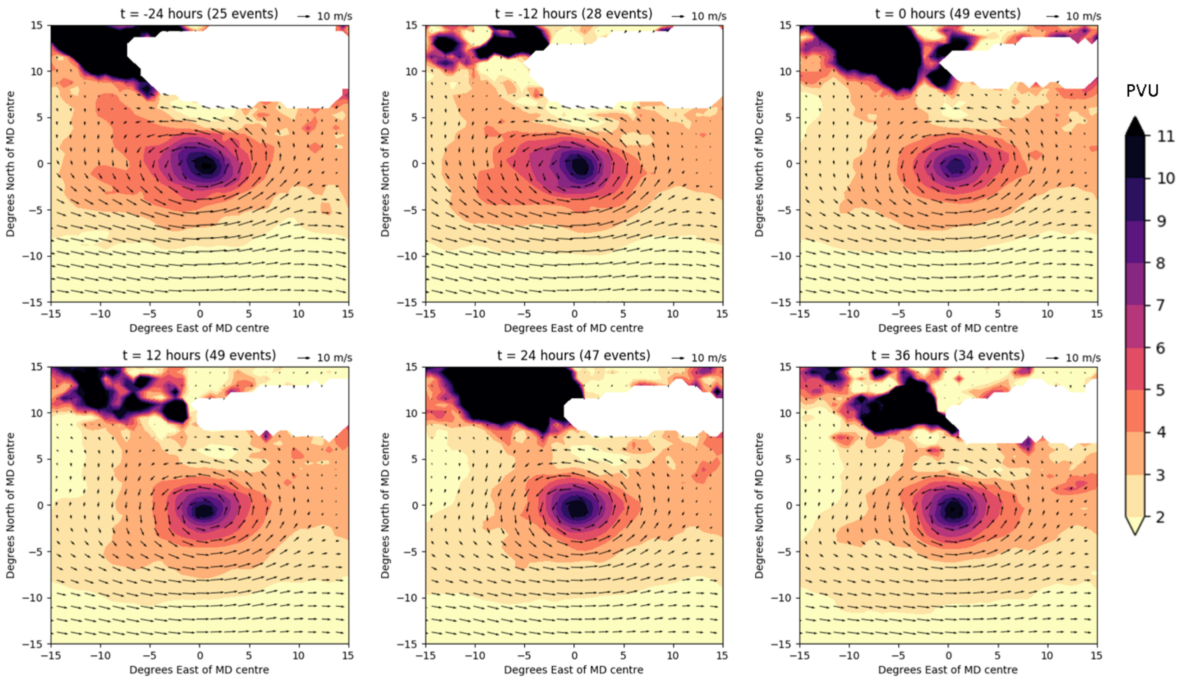

FIG. 11. Composites of 700 hPa potential vorticity [PVU] and horizontal winds centered on MDs with dry intrusions leading up to and after the interaction with the dry intrusion. *t* indicates the number of hours since the beginning of interaction with a dry intrusion. Locations where orography is below 3000 m for fewer than ten composite members are masked.

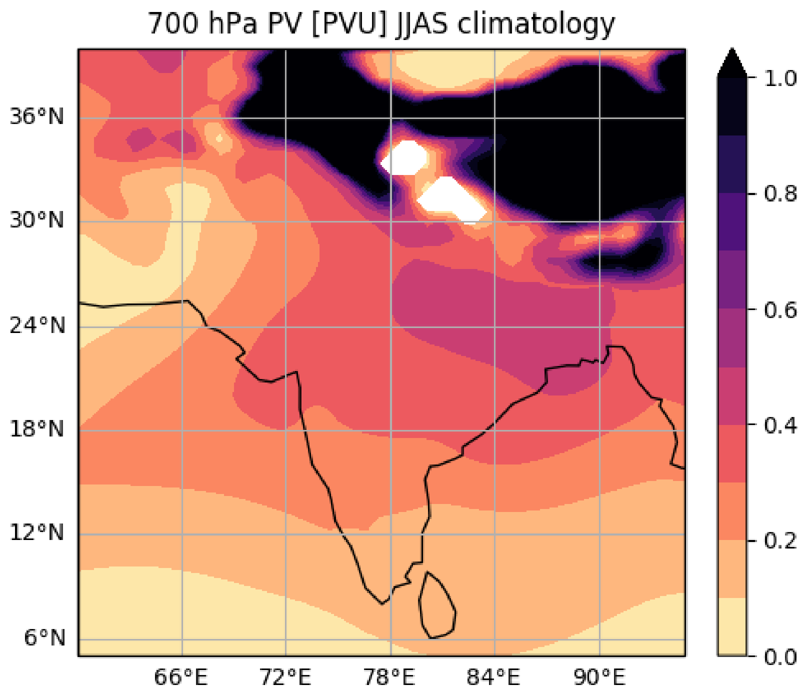

FIG. 12. Climatological potential vorticity at 700 hPa for June-September, from ERA-Interim.

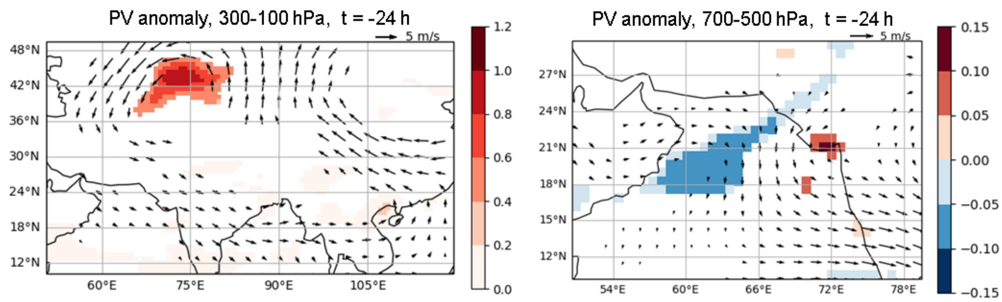

FIG. 13. Composite anomalies from climatology (PV and horizontal winds) 24 hours prior to MD-dry intrusion interactions, only shown where significant.

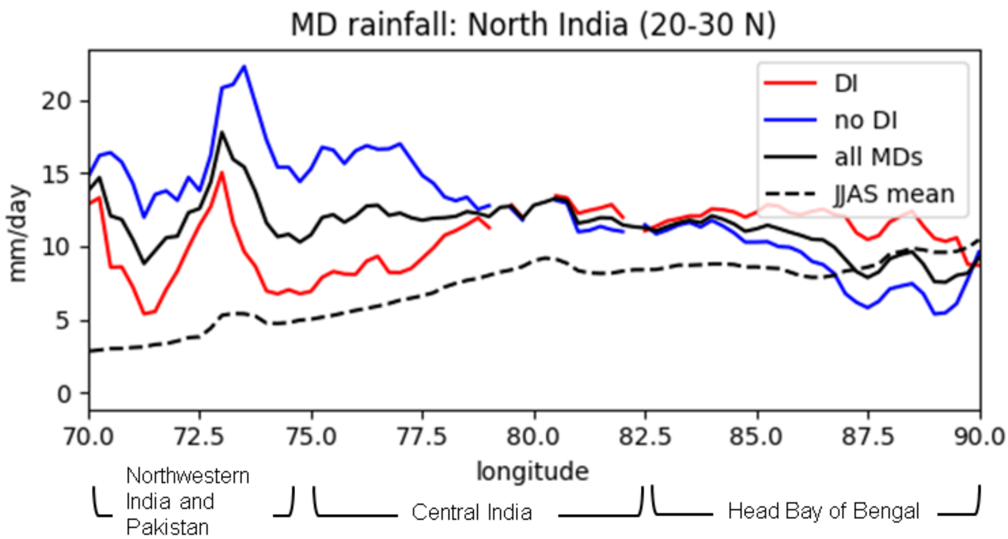

FIG. 14. Solid lines: time and meridional mean rainfall within 8 degrees of an MD center over land only, 20-30 N. The DI and noDI lines are only plotted where the difference between the two is statistically significant. Dashed line: time and meridional mean rainfall over land in June-September, 20-30 N.

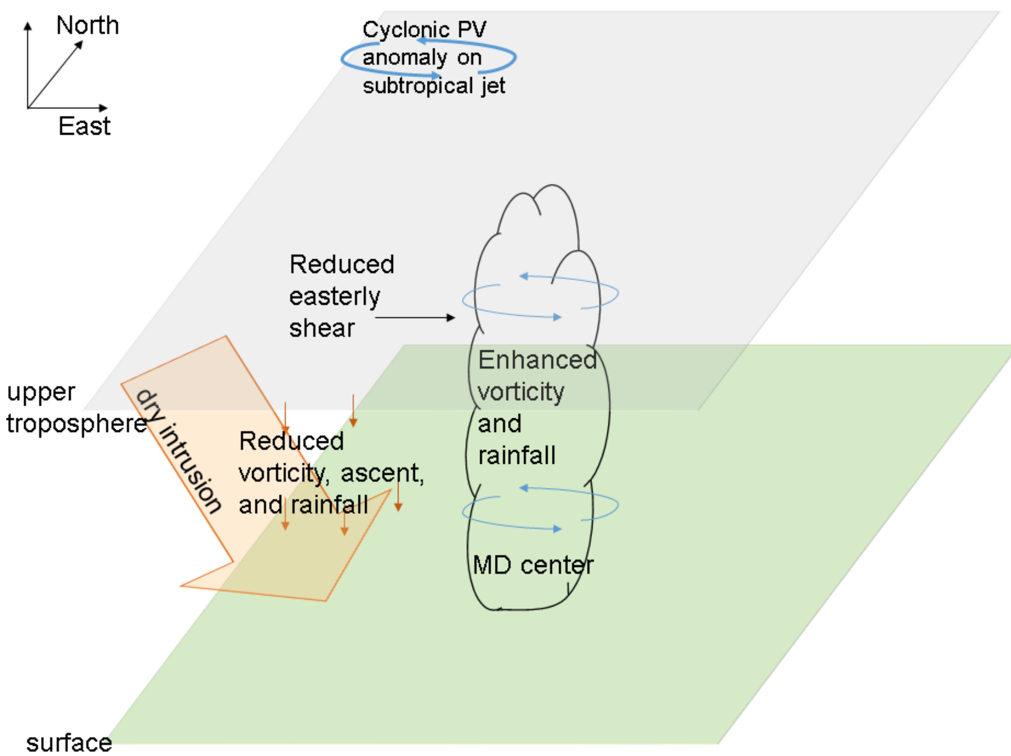

FIG. 15. Schematic of the interaction between an MD and a dry intrusion.